LA-UR-12-20666
Approved for public release; distribution is unlimited.

Title: A Survey of Detector Technologies for a First FFmF Experiment at MaRIE

Author(s): Kapustinsky, Jon S.

Intended for: Create citeable reference

Disclaimer:
Los Alamos National Laboratory, an affirmative action/equal opportunity employer,is operated by the Los Alamos National Security, LLC for the National NuclearSecurity Administration of the U.S. Department of Energy under contract DE-AC52-06NA25396. By approving this article, the publisher recognizes that the U.S. Government retains nonexclusive, royalty-free license to publish or reproduce the published form of this contribution, or to allow others to do so, for U.S. Government purposes. Los Alamos National Laboratory requests that the publisher identify this article as work performed under the auspices of the U.S. Departmentof Energy. Los Alamos National Laboratory strongly supports academic freedom and a researcher's right to publish; as an institution, however, the Laboratory does not endorse the viewpoint of a publication or guarantee its technical correctness.

A Survey of Detector Technologies for a First FFmF Experiment at MaRIE

Jon S. Kapustinsky, P25 Subatomic Physics, LANL, May 06, 2010

A Survey of Detector Technologies for a First FFmF Experiment at MaRIE

Jon S. Kapustinsky, P25, Subatomic Physics, LANL, May 6, 2010

Technology Scope. The performance requirements for detectors to be used for a possible first experiment at FFmF are challenging. One candidate for a first experiment, as proposed by Don Brown, is to image a 5 mm U02 sample using an x-ray beam with an energy spectrum between 75 and 350 keV. The x-rays will penetrate the sample with little or no divergence, so the beam will strike the detector at normal incidence. The detector should cover an area of at least 2 cm^2. The detector must have good spatial resolution, approximately 1-10 μm. A pixel detector array of 2048 x 2048 comprises roughly 4 million individual pixels in total. The charge collection time in the detector should be fast enough (on order ns's) to avoid excessive dead-time, and, therefore, unnecessary additional exposure to the background radiation. The readout time should be as fast as possible as this impacts the amount of time between useful beam buckets. The detector must have reasonable efficiency to detect 75-350 keV x-rays (>10^{-3}). And the detector must be able to survive the neutron and gamma ray radiation environment long enough to collect adequate data from the sample (@4m 1.27E+9 n/mA/s/cm2, @4m 2.50E+8 gamma/mA/s/cm2).

The list of detector technologies that meet some of these requirements is fairly extensive. Some of the standard x-ray detector technologies are listed in the Thompson x-ray data booklet [1] shown in figure 1. It should be noted, there are no detector systems in operation today, at least that were found as a result of this survey, that meet all of the requirements for the first FFmF experiment as presently defined. One big challenge is the combination of state-of-the-art imaging performance coupled with the demanding metric for radiation hardness. A second challenge is to detect very hard x-rays (>40 keV) with the required spatial resolution. The most promising of the technologies identified within this survey will be grouped into the following categories, a) those that need some evolutionary development, b) need extensive evolutionary development, or 3) need to make a revolutionary leap from present day performance to be of use.

Table 4-2. Properties of common x-ray detectors; ΔE is measured as FWHM.

Detector	Energy range (keV)	ΔE/E at 5.9 keV (%)	Dead time/event (μs)	Maximum count rate (s^{-1})
Gas ionization (current mode)	0.2–50	n/a	n/a	10^{11}[a]
Gas proportional	0.2–50	15	0.2	10^6
Multiwire and microstrip proportional	3–50	20	0.2	$10^6/mm^2$
Scintillation [NaI(Tl)]	3–10,000	40	0.25	2×10^6
Energy-resolving semiconductor	1–10,000	3	0.5–30	2×10^5
Surface-barrier (current mode)	0.1–20	n/a	n/a	10^8
Avalanche photodiode	0.1–50	20	0.001	10^8
CCD	0.1–70	n/a	n/a	n/a
Superconducting	0.1–4	< 0.5	100	5×10^3
Image plate	4–80	n/a	n/a	n/a

[a] Maximum count rate is limited by space-charge effects to around 10^{11} photons/s per cm^3.

Figure 1. X-ray detectors and their properties**.**

X-ray interaction. There are three ways that x-rays generally interact with matter:

1) At the lowest energies, up to a few keV, x-ray interactions with detector materials are predominantly through the photoelectric effect. In this process, an x-ray interacts with an electron that is bound to an inner atomic orbital. The x-ray is absorbed and a free electron is created with kinetic energy that is approximately equal to that of the incident x-ray.

2) At higher energies, from 10-40 keV, Compton scattering becomes increasingly important and then dominant above 100 keV. In the Compton process, the x-ray elastically scatters from a free or loosely bound electron, and transfers a portion of its energy into the kinetic energy of the electron. What is important to note for the discussions to follow, is that the amount of energy that is transferred to the electron is continuous from nearly zero up to almost the entire energy of the incident x-ray.

3) At the highest energies, above the threshold value 1.022 MeV, production of electron–positron pairs become the important conversion mechanism.

Scintillator plus optically coupled-CCD, phosphors and single crystals. For high spatial resolution applications using x-rays, the predominant technology choice for synchrotron experiments is some type of x-ray sensitive scintillator used as converter, and coupled to a high resolution CCD. There are two basic classes of scintillator that are commonly used, single crystal scintillators and phosphors.

Thin phosphor sheets are used to covert x-rays into visible light, and the visible light is optically coupled to a pixel CCD. The CCD converts the light to an electronic signal and maintains the accuracy of the position of the light flash. The intrinsic spatial resolution of the phosphor itself depends on the thickness of the sheet, and worsens with thicker sheets. Resolution is very roughly proportional to half the phosphor thickness [2]. Sheets are currently commercially fabricated down to 1 μm thick. Conversely, the efficiency of x-ray conversion in the phosphor increases with sheet thickness. So, a balance between the two must always be struck.

Table 1. A survey of characteristics of selected phosphor materials [6, 7, 12, 13, 18, 89].

Phosphor	Density (g cm^{-3})	Decay time (ns)	Efficiency η (%)	Emission maximum (nm)	Afterglow
ZnS:Ag	3.9	~1000	17–20	450	Very high
$CaWO_4$	6.1	6×10^3	5	420	Very low
Gd_2O_2S:Tb	7.3	6×10^5	13–16	540	Very low
Gd_2O_2S:Pr, Ce, F	7.3	4000	8–10	490	Very low
LaOBr:Tb	6.3	~10^6	19–20	425	Low
$YTaO_4$:Nb	7.5	~2000	11	410	Low
Lu_2O_3:Eu	9.4	~10^6	~8	611	Medium
$SrHfO_3$:Ce	7.7	40	2–4	390	Not reported

Table 1. A partial list of x-ray conversion phosphors. [3]

In a review paper on scintillators for x-rays, Nikl lists some of the more important characteristics ascribed to a good x-ray conversion phosphor [3]:

1. Robustness and stability;
2. X-ray stopping power;
3. Spectral matching of the light output to the next optical relay element;
4. **Energy efficiency for conversion of x rays to light;**
5. Luminescent decay time and afterglow;
6. Linearity of light output with incident x-ray dose and intensity;
7. Noise; and
8. Spatial resolution across the screen. [Nikl]

The phosphor YAG:Ce ($Y_3Al_5O_{12}$:Ce) meets many of the criteria listed above and it used extensively in x-ray imaging. Koch recently reported on an analysis he did for three experimental configurations at the LCLS using YAG:Ce phosphors of 1 μm and

5 μm thickness and a 1 μm thick LSO:Ce phosphor. He claims that sub-micron resolution is obtainable for both of the thinner phosphors. In his work, the phosphors are coupled to a Photometrics CH250 14-bit CCD with 1024^2 pixels, $(24\ \mu m)^2$ pixel size. The readout time of the CCD is 5 s. The performance details are listed in table 2.

Detector Design	Resolution (fw90%int) (μm) [Eq. (3a)]	X-Ray Energy (keV)	Absorption Efficiency	DQE [Eq. (8)]
Existing				
5-μm YAG:Ce	1.5	14	0.04	0.026
NA = 0.55		30	0.04	0.032
Design				
1-μm YAG:Ce	0.8	14	0.008	0.0069
NA = 1		30	0.006	0.0056
1-μm LSO:Ce	0.8	14	0.08	0.066
NA = 1		30	0.01	0.0091

Table 2. Performance parameters for three experimental configurations at the LCLS using a YAG:Ce phosphor and a Photometrics CH250 14-bit CCD [3].

At the High Energy Beamline 1D15A at the European Synchrotron Radiation Facility (ESRF) the experimental team has developed a fast three dimensional x-ray microtomography system that uses YAG:Ce and LAG ($Lu_3Al_5O_{12}$:Eu) phosphors. Some of the relevant properties of these phosphors are listed in table 3 [4]. The experimental setup of 1D15A is shown in figure 2. Two configurations are available: a low resolution and a high resolution. The low resolution setup is for samples of 10-20 mm and uses a 250 μm YAG:Ce phosphor. The high resolution setup is for samples of 1-2 mm and uses LAG phosphors of 1 μm, 6μm and 26 μm. The best reported resolution is 2 μm. Samples are continuously rotated at a constant speed while the radiographs are acquired. Intermediate magnifying optics allow the CCD to be placed in a position where it can be shielded from the beam. The CCD camera used is a DALSTAR 1M60 consisting of 1024 x 2048 pixels, $(14 \times 14\ \mu m)^2$.

	Low resolution	High resolution
Scintillator	YAG:Ce ($Y_3Al_5O_{12}$:Ce)	LAG ($Lu_3Al_5O_{12}$:Eu)
Substrate	None	YAG (170 μm)
Active layer thickness	250 μm	1–6–26 μm
Spectral emission	550 nm	500–800 nm
Density	4.6 g/cm^3	6.6 g/cm^3
Decay time (1/e intensity)	70 ns	7 ms

Table 3. Phosphors used on 1D15A at the ESRF [4].

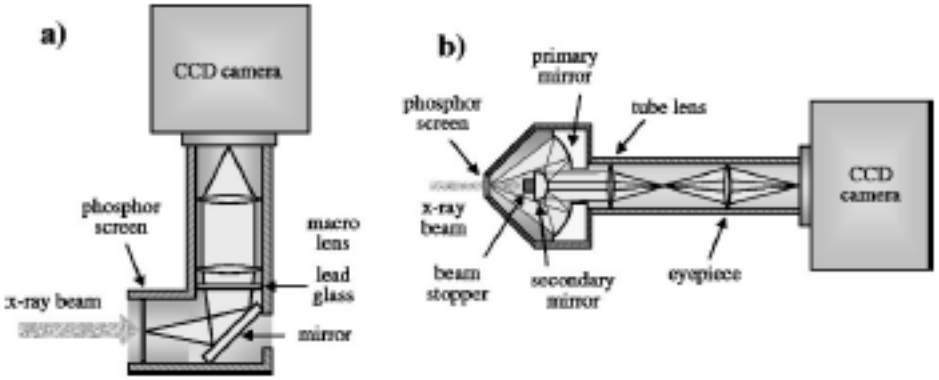

Figure 2. a) low resolution and b) high resolution configuration [4]

The x-ray spectrum at the 1D15A beamline is 20-250 keV, very much is in the region of interest for FFmF applications. The higher energies lead to the use of thicker phosphors, up to 250 μm. The experimental station is located about 65m from the source. To get sufficient photon flux, the experiment takes a white beam. The beam spectrum is shown in figure 3. The total acquisition time to characterize a sample is from a few seconds up to 1 minute.

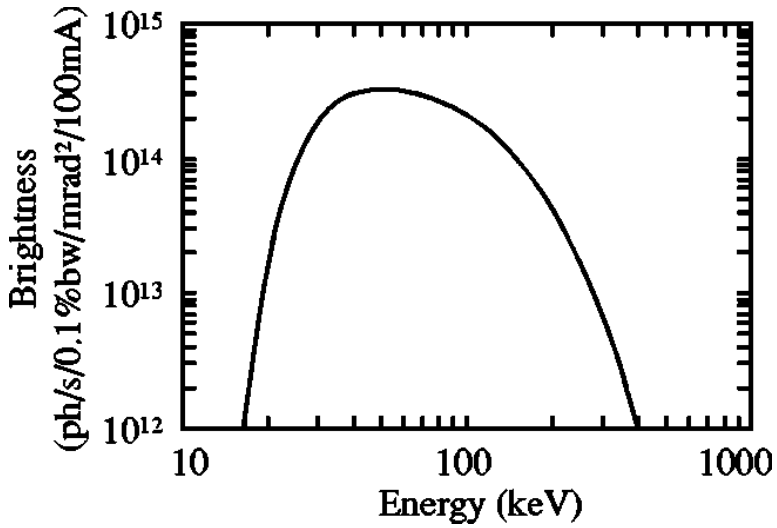

Figure 3. ID15 x-ray spectrum after attenuators when operating the asymmetric multi-pole wiggler with the maximum magnetic field strength (1.84 T) [4].

A phosphor/CCD detector system such as the two that are described above meets the spatial resolution requirements of a first experiment at the FFmF, but only at the lower end of the beam energy. The 1D15A author, Michieli, reports that even thinner phosphors are under investigation in order to improve the spatial resolution, which will cut even further into the conversion efficiency at the high end of the beam energy spectrum.

An alternative approach to deal with some of the limitations of thin phosphor screens has been suggested by Nikl, in his review paper on scintillation detectors for x-rays. [3] As an alternative, Nikl examines single crystal scintillating material. He emphasizes the point that the need for high spatial resolution (thin screen) and high x-ray stopping power (thick screen), are contradictory requirements and that this is also true in the case of single crystalline thin film/plate screens used for the high resolution 2D-imaging. In addition to loss of spatial resolution, the cost of improving conversion efficiency by going to thicker screens means that the amount of light available at the external photodetector is diminished due to multiple light scattering. Nikl suggests that a virtual breakthrough has come with the fabrication of long (up to 1–2 mm) ordered and densely packed needles of CsI-based scintillators. The needles act like miniature light guides and can maintain high spatial resolution even with the layer thickness exceeding 1 mm, resulting in high x-ray stopping power as well as good resolution. Such columnar CsI structures are shown in figure 4.

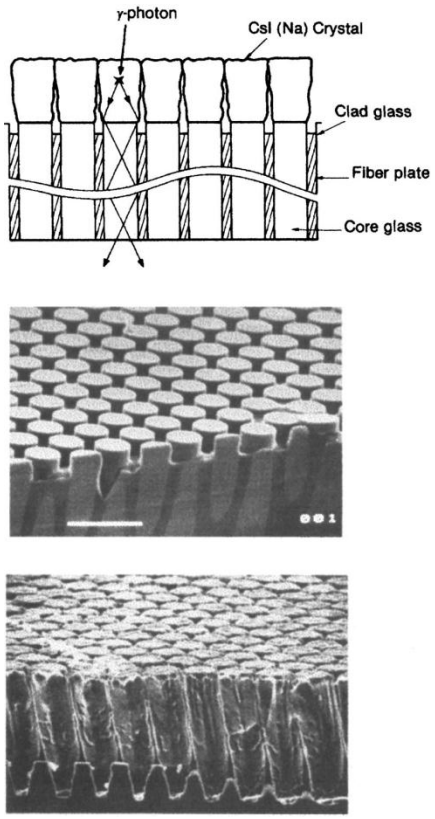

Figure 4. CsI:Na phosphor grown in columns on an etched fiber-optic plate top panel. A micrograph of the plate before phosphor deposition, but after fiber matrix etching, is shown in the middle panel and after phosphor deposition in the bottom panel. [5]

Nikl's list of the characteristics of a good quality crystal scintillator is slightly different than his list for the phosphor [3]. For scintillators, the importance of light yield is equivalent to the conversion efficiency metric for phosphors. The most commonly used crystal scintillators are listed in table 4 below.

(1) **Light yield,**
(2) X-ray stopping power,
(3) Scintillation response—decay time,
(4) Spectral matching between the scintillator emission spectrum and photo-detector,
(5) Chemical stability and radiation resistance and
(6) Linearity of light response with the incident x(γ)-ray photon energy—energy resolution.

Crystal	Density (g cm^{-3})	Light yield (photon MeV^{-1})	Dominant scintillation decay time (ns)	Emission maximum (nm)	$\Delta E/E$ at 662 keV (%)
CsI:Tl	4.51	66 000	800	550	6.6
NaI:Tl	3.67	41 000	230	410	5.6
$LaBr_3$:Ce	5.3	61 000	35	358	2.9
K_2LaI_5:Ce	4.4	55 000	24	420	4.5
BaF_2 (only cross luminescence)	4.88	1 500	0.6–0.8	180–220	7.7
$Bi_4Ge_3O_{12}$	7.1	8 600	300	480	9.0
$PbWO_4$	8.28	300	2–3	410	30–40
$CdWO_4$	7.9	20 000	5 000	495	6.8
$YAlO_3$:Ce	5.6	21 000	20–30	360	4.6
$LuAlO_3$:Ce	8.34	12 000	18	365	~15
$Y_3Al_5O_{12}$:Ce	4.56	24 000	90–120	550	7.3
$Lu_3Al_5O_{12}$:Ce	6.67	12 500	55	530	11
Gd_2SiO_5:Ce	6.7	8 000	60	420	7.8
Lu_2SiO_5:Ce	7.4	26 000	30	390	7.9

Table 4. Properties of single crystal scintillators [3].

A large plate of columnar CsI crystal scintillator can be coupled to a CCD or to a high resistivity silicon pixel array. An amorphous silicon pixel array is shown for example in figure 5. A nice feature of the design shown in figure 6 is that the electronics are placed around the periphery where there is some chance of shielding them from the radiation environment.

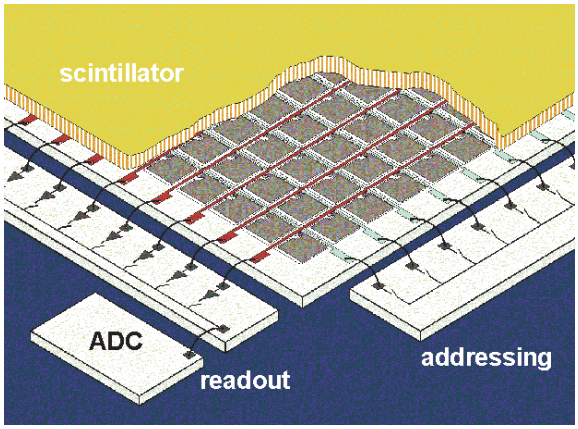

Figure 5. Schematic of a flat-panel detector. An array of amorphous-silicon diodes positioned on a glass plate is covered by a scintillator screen of columnar grown CsI:Tl. Addressing lines and readout lines are respectively coming from and going to chips at the edge of the plate [3].

The absorption efficiency as a function of photon energy is shown in figure 6. At 2 mm thickness, a CsI crystal is 20% efficient for a 300 keV photon. The wavelength of the scintillation light from CsI is 550 nm. The quantum efficiency of a high quality CCD (see 1D15A reference below) at that wavelength is approximately 15%. See figure 7. The penetration depth of 550 nm light in high resistivity silicon is on the order of 5-10 μm, giving the CCD a clear advantage in light detection. However, the

advantages that a high resistivity silicon detector has over conventional CCDs are readout speed, and improved radiation hardness. The relative radiation hardness of these materials will be discussed in detail in a subsequent section.

Figure 6.
Absorption Efficiency of CsI

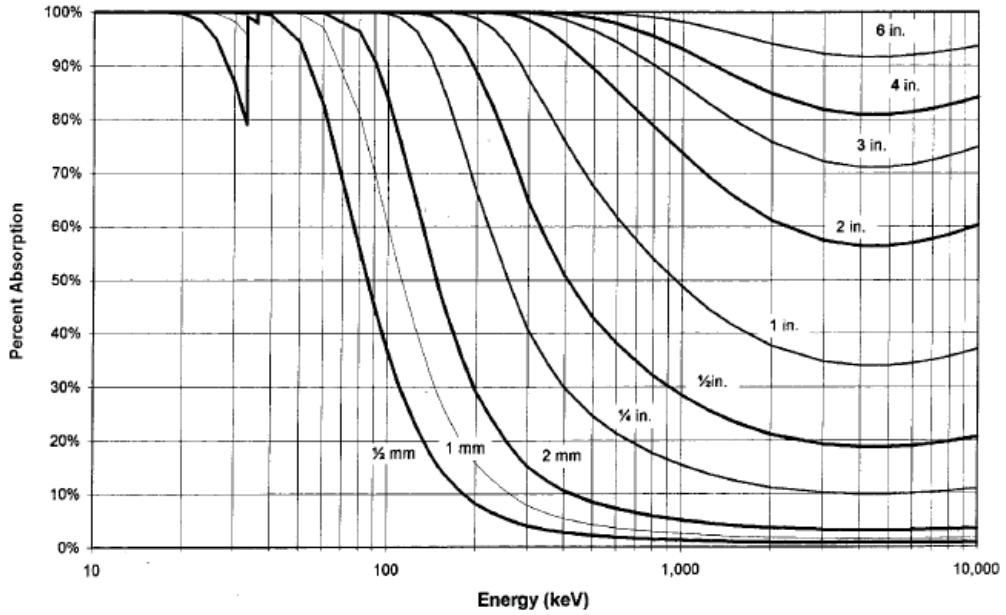

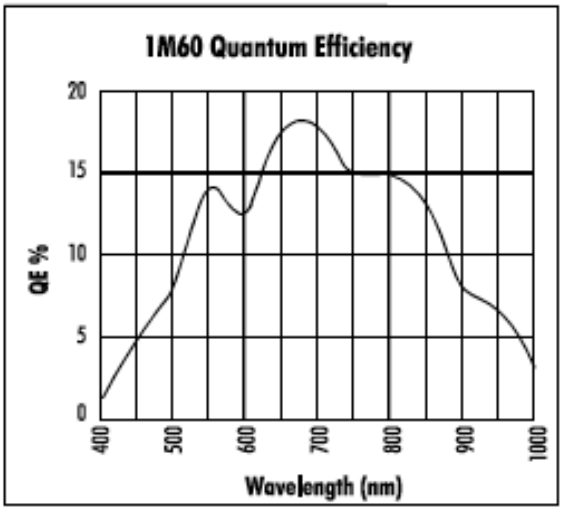

Figure 7. CCD quantum efficiency versus wavelength from Speiler [6].

Henning Poulsen from RISØ has proposed an interesting variant on Nikl's concept. He describes a three-dimensional X-ray detector for micro-imaging with 30–200 keV photons. It comprises a set of semi-transparent structured scintillators,

whereby each scintillator is a regular array of CsI waveguides fabricated in pores that are etched in a silicon substrate [7]. The micro-structured scintillator elements are a few μm in diameter. Poulsen states that with this concept, demonstrated using currently available hardware, one can achieve a spatial resolution of 1 μm. Only the pitch of the waveguides determines the resolution of a single screen, not the thickness. In comparison with conventional homogeneous screens, an improvement in efficiency by a factor of 5–15 is obtainable. The cross-talk between screens in the three-dimensional detector is shown to be negligible. The concept is shown in figure 8. The estimated improvement in efficiency over unstructured scintillator is plotted in figure 9. Resolution for a pitch of 1 μm and 4 μm is plotted in figure 10.

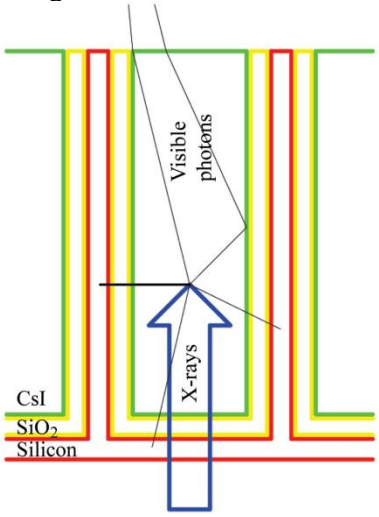

Figure 8. Schematic of a structured scintillator showing an absorption event and the internal reflection of secondary emitted photons [7].

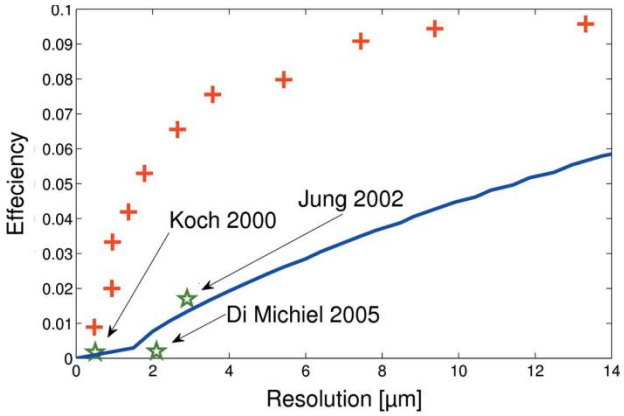

Figure 9. Efficiency versus resolution (R90W) for an unstructured scintillator (solid line) and a structured scintillator (crosses). For comparison, experimental points are inserted (stars) from Jung et al. (2002), Di Michiel et. al. (2005) and Koch et al. (2000) [7].

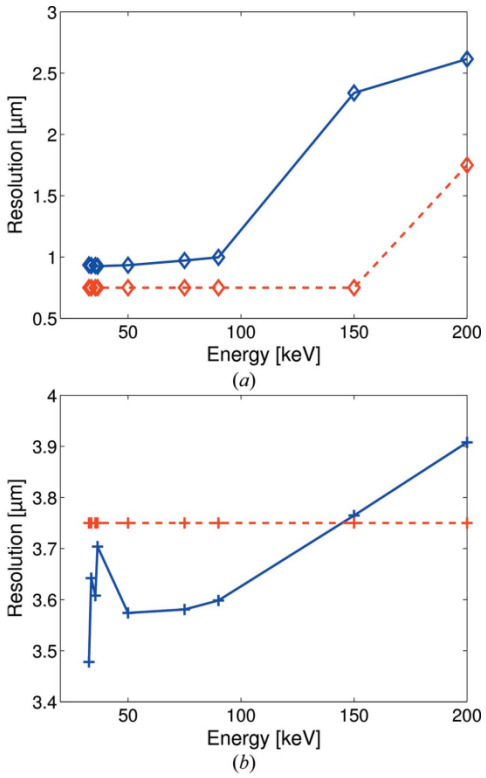

Figure 10. Resolution as a function of the X-ray energy for pitches of (a) 1 μm and (b) 4 μm. Solid lines are R90W and dashed lines are FWHM measures [7].

Semiconductor as converter. Sol Gruner's group at Cornell has been working on next generation detectors for synchrotron applications for years, often in collaboration with Argonne National Lab. Gruner believes that semiconductor converters have significant advantages over phosphors. Semiconductors directly convert the x-ray energy into electrical charge, which often simplifies the design of the detector. The physics of x-ray absorption and electron-hole production in a semiconductor is generally simpler and, therefore, better understood than light production in phosphors. Compared to phosphor converters, semiconductors are also usually much more efficient, resulting in more charge carriers, are more linear and less noisy, and the charges are more rapidly and more efficiently collected. The disadvantages of semiconductors that have limited their use as x-ray converters is that thick detectors are hard to make, and the semiconductor of choice, namely silicon, has relatively low stopping power [5].

In his Doctoral dissertation at Cornell, Daniel Schuette describes in great detail the development of the Mixed–Mode Pixel Array Detector, a new type of semiconductor imaging detector for synchrotron based x-ray science that was developed by Gruner's group [8]. An artist's rendering is shown in figure 11. The detector is

comprised of two elements, an array of p-n junction diodes fabricated on high resistivity silicon, and individual pixel readout electronics designed in CMOS. These two are connected via bump bonds. Because the Analog PAD front end integrates currents, only the bias current of the integration stage amplifier limits the maximum flux per-pixel, allowing the Analog PAD to have very high per-pixel flux tolerance. The detector is designed for readout times of less than 1 ms, a dynamic range extending from single x-rays to a full well of more than 2.6 x 10^7 x-rays/pixel, capable of measuring fluxes up to 10^8 x-rays/pixel/s, with a sub-pixel point spread. Schuette claims that these characteristics exceed, by orders of magnitude, the capabilities of the current generation of x-ray imagers. The detector specifications are listed in table 5. Figure 12 shows a drawing of what an array of detectors might look like as conceived for the LCLS. Table 6 contains a list of several PAD detectors that have been developed around the world. All x-ray related parameters in the table are based on a 10 keV beam.

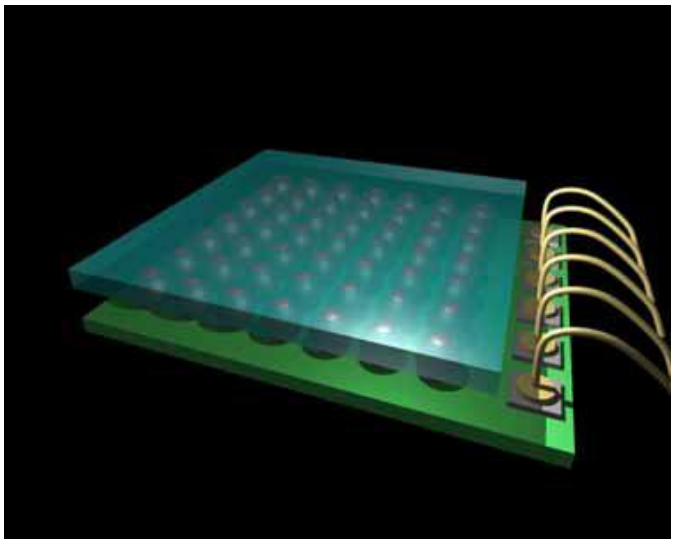

Figure 11. Artist's conception of a Pixel Array Detector (PAD) illustrating: the detector diode layer, responsible for converting photons into electrical charge; the signal processing application specific integrated circuit (ASIC) layer, responsible for processing the signal generated by the detector diode; and the array of bump bonds that provide electrical interconnects between corresponding pixels on the diode layer and the ASIC [8].

Detector Format	Multi-Mosaic of PAD Hybrids
Single PAD Hybrid Format (ASIC)	128×128 pixels
Pixel Size	150 μm × 150 μm
Framing Rate	1,000 Hz
Readout Time	< 1 ms
Read Noise	0.4 x-rays/pixel
Well Capacity	2.6×10^7 x-rays/pixel
Maximum Flux	$> 1.0 \times 10^8$ x-rays/s/pixel

Table 5. Pixel Array Detector specifications [8].

For comparison: Detectors at LCLS (120 Hz!)

S. Boutet
(CXI instrument)

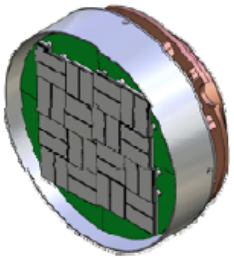

- 2D Pixel Array Detector
  - High resistivity Silicon (500 µm) for direct x-ray conversion.
  - Reverse biased for full depletion.
  - Bump-bonding connection to CMOS ASIC.
- <1 photon readout noise
- 110x110 µm^2 pixels
- 1520x1520 pixels
- 10^3 dynamic range
- 120 Hz readout
- **Tiled detector, permits variable 'hole' size**

Collaboration with the Gruner Group at Cornell University

A. Robert
(XCS instrument)

- 2D Pixel Array Detector
- <<1 photon readout noise
- 55x55 µm^2 pixels
- 1024x1024 pixels
- 10^2 dynamic range
- 120 Hz readout
- **More modules, tiled detector**

Collaboration with P. Siddons at BNL

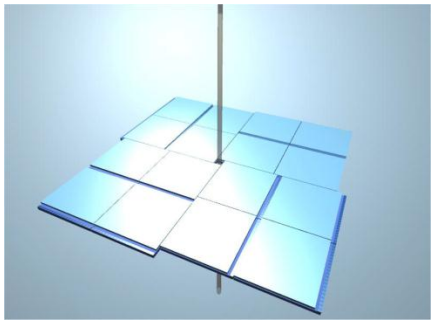

Figure 12. A mosaic of Pixel Array Detectors as envisaged for the LCLS [8, 9].

	Medipix–2	Pilatus	XPAD3	LAD	Cornell 100 × 92	LCLS
PAD Method	Digital	Digital	Digital	Digital	Analog	Analog
Pixel Size [μm^2]	55 × 55	172 × 172	130 × 130	150 × 150	150 × 150	110 × 110
Read Noise [x-rays/pixel]	< 1	< 1	< 1	< 1	~ 2.6	0.2/1.3
Read Time [ms]	3	3	2	0.4	$\sim 10^3$	< 6
Well-Depth [x-rays/pixel]	2^{14}	2^{20}	2^{12}	2^{15}	$\sim 1.7 \times 10^4$	300/2,250
Max. Flux [x-rays/pixel/s]	2×10^6	$< 8 \times 10^6$	$\sim 10^6$	$\sim 10^6$	10^{12}	$> 1 \times 10^{15}$
References	[48]	[17, 71, 22]	[73, 12]	[30]	[83]	[76]

Table 6. A list of some prominent PAD projects. Performance numbers are based on a 10 keV beam [8].

Another variant on the PAD concept is the pnCCD, originally developed for space applications for the XMM space mission. Struder of the Max Planck Advanced Study Group has been leading the development of the concept for 4th generation x-ray sources. [10]. The experimental setup he reports on, CAMP, was installed at the LCLS in November 2009. See figure 13. The pnCCD is another device that makes use of high resistivity silicon for the direct conversion of incident x-rays. It shares many similarities, in terms of operation with the Gruner Pad module. The main difference is smaller pixel size and a larger array, comprised of 2048 x 2048 pixels. The framing rate is, therefore, slower than the Gruner Pad array. The readout chip is a commercially available ASIC called the CAMEX. The properties of the CAMP pnCCD are listed in table 7. A photograph of a test pnCCD is shown in figure 14 and test results of the quantum efficiency versus energy are shown in figure 15, showing a significant roll-off above 20 keV.

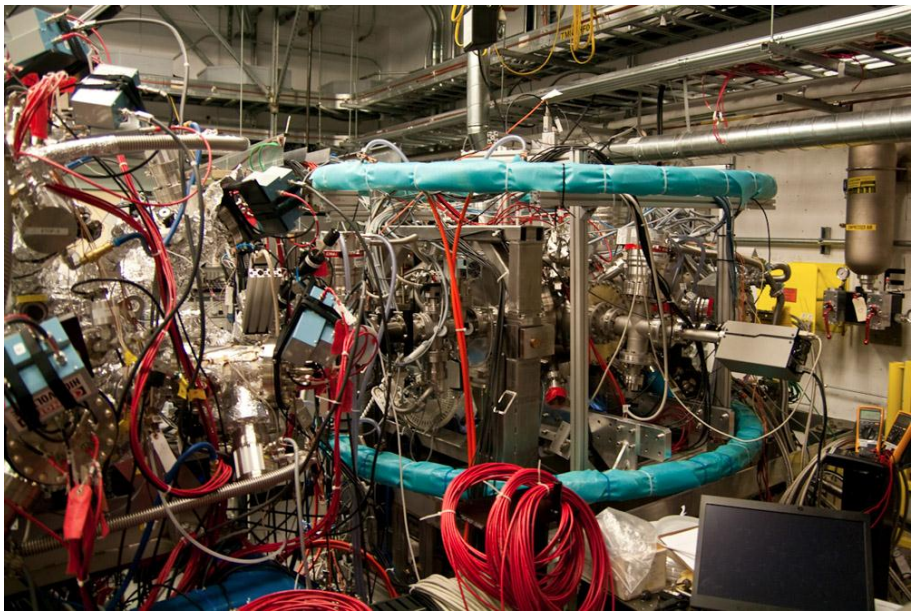

Figure 13. CAMP installed at the LCLS.

Parameter	2-D imager requirements for FLASH, LCLS, SCSS and XFEL requested by the user community	pnCCD properties
Single photon resolution	Yes	Yes
Energy range	0.05–24 keV	0.05–25 keV
Signal rate/pixel/bunch	10^3 (10^5)	10^3 at 2 keV
Charge handling capacity	—	Approx. 5×10^5 electrons per pixel
Quantum efficiency	> 0.8	> 0.8 from 0.3–12 keV
Number of pixels, format	512×512 (min.)	1024×1024 and 2048×2048
Pixel size	$< 100 \times 100\ \mu m^2$	$75 \times 75\ \mu m^2$
Frame rate repetition rate (except XFEL's 5 MHz operation)	5–120 Hz	Continuous up to 200 Hz
Externally triggerable	—	Yes
Integrated center hole	Ø3 mm	Ø2.4 mm
EUROPEAN XFEL burst mode	5 MHz (3000) bunches	Not applicable
Readout noise	< 150 electrons	20 e^- (low gain), 2 e^- (high gain)

Table 7. List of pnCCD properties [10].

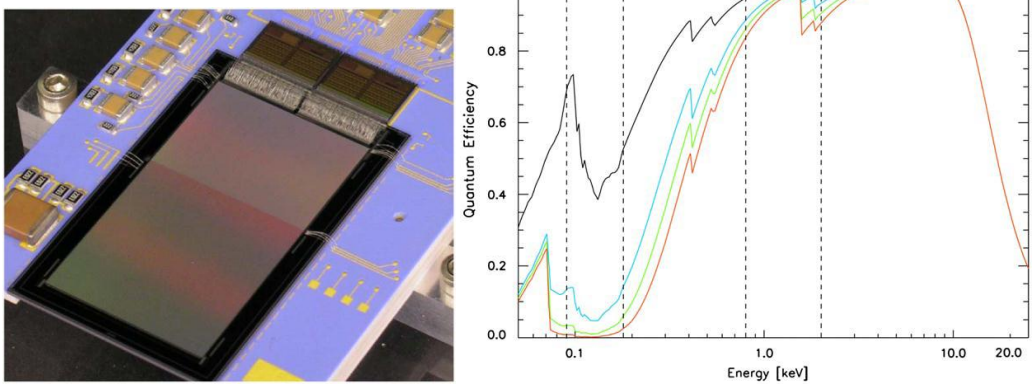

Figures 14 and 15. A test pnCCD with 256 x 512 pixels and CAMEX chip readout is shown on the left. The quantum efficiency versus energy for a variety of filters is plotted on the right [10].

Double-sided silicon microstrips. Silicon microstrips on high resistivity material can be implanted at widths of approximately 8 μm on approximately 18 μm pitch. The crossing of two orthogonally oriented strips forms a virtual pixel of 18 μm^2. Strips can be patterned on each side of a silicon detector with one side patterned in the x-direction and the other side patterned in the y-direction. One side collects electrons, and one side collects holes. This geometry provides the possibility to get all the CMOS electronics moved to the perimeter of the detectors, and perhaps to a lower radiation field or to a location where they can be shielded. The concept is illustrated in figure 16.

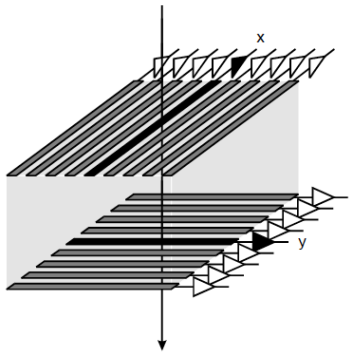

Figure 16. Silicon microstrips placed orthogonally.

3D silicon detectors Piemonte. The interest for 3D detectors is continuously growing because of their intrinsic capability to control the depletion mechanism by acting on the layout of the vertical electrodes only. [11, 12] By properly designing the electrodes' width and pitch, the sensor designer can obtain depletion voltages two orders of magnitude lower than those of standard planar detectors (~10V), and collection time one order of magnitude lower (~1ns). The vertical electrodes are on order of 5 μm in diameter. These detectors have become prime candidates for the anticipated upgrade project for the Super-LHC because of their inherent radiation hardness. Piemonte's particular design, one among many recently proposed, has emerged as a leading candidate in the CERN detector R&D community because it minimizes the fabrication process complexity, so that 3D detectors can be produced in large volumes with a good yield and at accessible costs. There are two main drawbacks to these devices: (a) columnar electrodes are dead regions, (b) the regions located in the middle between electrodes of the same type present a null-field, thus delaying the collection of carriers generated in such zones which slowly move by diffusion until they reach a region with a sufficient electric field. These do not seem to be fatal flaws for an FFmF experiment. The concept is shown in figure 17. A microphotograph of 250 μm vertical electrodes in a device produced by SINTEF is shown in figure 18.

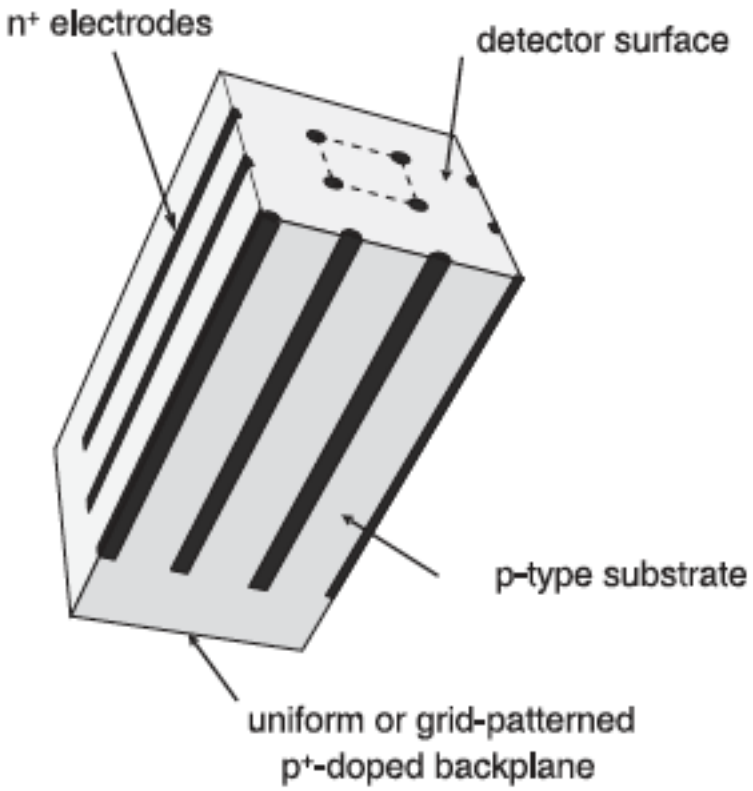

Figure 17. Piemonte's 3D detector concept [12].

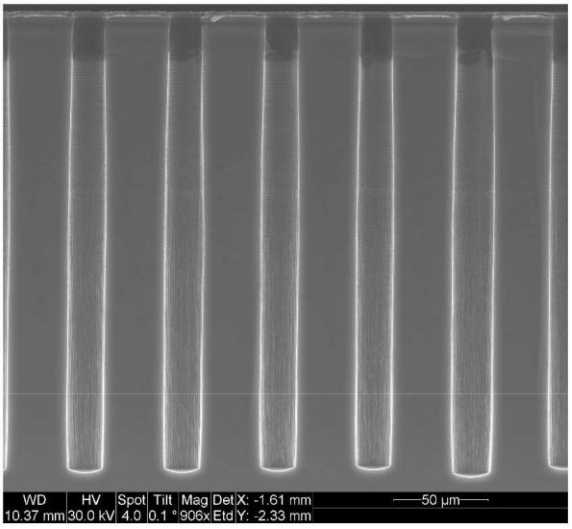

Figure 18. Microphotograph of 3D electrodes in a SINTEF device [13].

Compton conversions in high resistivity silicon. The limitation that all detectors based on high resistivity in terms of stopping power was stated above. If it were only a problem of low conversion efficiency, one could compensate with longer runs.

The drop off in efficiency for a commercially available diode is shown in figure 19. The efficiency for a 500 μm thick silicon detector is tolerable above 100 keV, and detectors of 2 mm are being fabricated today. Detectors could also be stacked. Ten 2 mm-thick silicon detectors stacked would be approximately 50% efficient for x-rays up to 40 keV (see figure 20). The greater problem lies in the Compton process itself, especially above approximately 30 keV incident x-ray energy where it becomes a significant fraction of all conversions. As stated earlier, the secondary electron produced in a Compton interaction can acquire any value of energy from a minimum, up to almost the entire energy of the incident x-ray. Multiple scattering of electrons within the silicon at these energies could degrade the measured point resolution of any silicon detector that operates in the Compton regime. This is an effect that has to be modeled in detail for all high resistivity detectors.

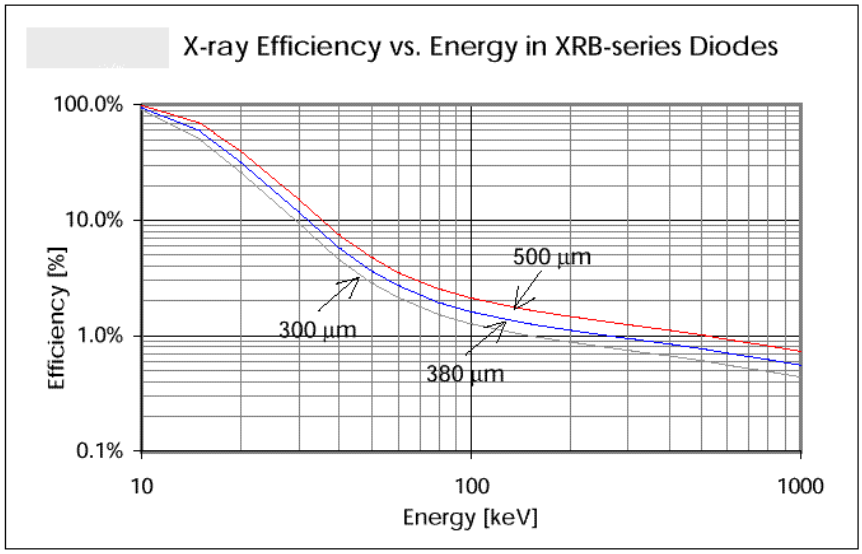

Figure 19. Efficiency versus incident energy in a silicon diode [14].

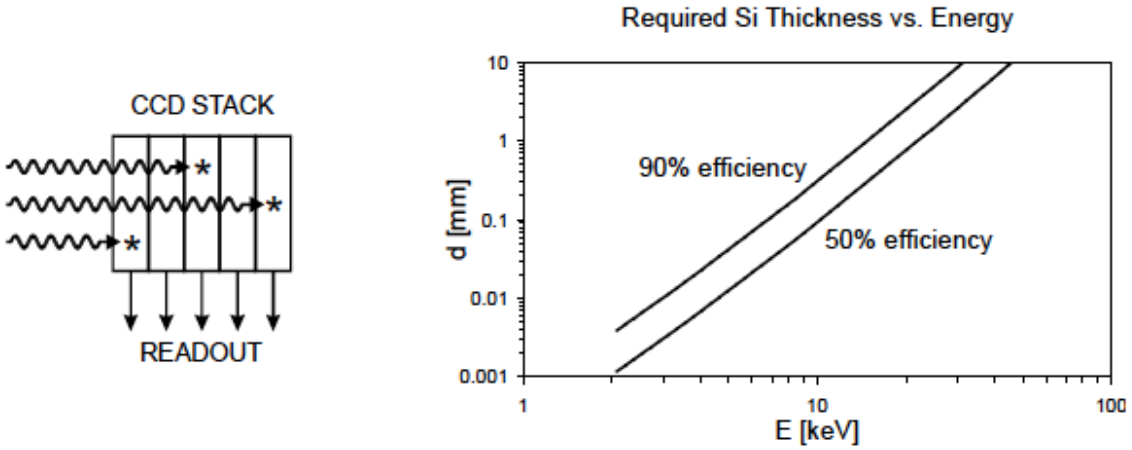

Figure 20. Silicon efficiency versus energy, a stacked solution. [6]

Other Detectors for the XFEL. The DEPFET-APS LPD and AGIPD consortia have been given the challenge to build pixel area detectors for the European XFEL. The basic concepts and parameters of these detectors are summarized in table 9. At present, these designs do not seem to directly address the fundamental specifications required for the FFmF experiment, as they are all designed for much coarser spatial resolution.

Table 3: Concepts of the three different XFEL pixel detector projects.

	DEPFET-APS	LPD	HPAD
# of pixels	$1\,\mathrm{k} \times 1\,\mathrm{k}$	$1\,\mathrm{k} \times 1\,\mathrm{k}$	$1\,\mathrm{k} \times 1\,\mathrm{k}$
Pixel size	$200\,\mu\mathrm{m} \times 200\,\mu\mathrm{m}$	$500\,\mu\mathrm{m} \times 500\,\mu\mathrm{m}$	$200\,\mu\mathrm{m} \times 200\,\mu\mathrm{m}$
Sensor	DEPFET array	Si-pixel	Si-pixel
Dynamic range	$\geq 10^4$ ph	2×10^4 ph (10^5 ph)	$\geq 2 \times 10^4$ ph
Noise	$\approx 15 \times 10^{-3}$ ph ≈ 50e	≈ 0.21 ph (≈ 0.93 ph) $\approx 700\,\mathrm{e}$ ($\approx 3100\,\mathrm{e}$)	$\approx 45 \times 10^{-3}$ ph $\approx 150\,\mathrm{e}$
Concept	DEPFET nonlinear gain compression Per-pixel ADC	Multiple gain paths On-chip ADC	Adaptive gain switching (preset gain option)
Storage	8bit DRAM	3-fold analogue	2 bit digital + analogue
Storage depth	≥ 256	512	≥ 200
Challenges	Linearity & calibration In-pixel ADC DRAM refresh Power budget Pixel area	Preamplifier: noise, dynamic range & PSRR Analogue storage	Dynamic gain switching Charge injection Analogue storage Pixel area
	Radiation hardness		

Table 9. [15] Three concepts for the XFEL.

Diamond-based detectors. Diamond as a potentially very radiation hard material, roughly one order of magnitude harder than high resistivity silicon, has been explored intensively by the R&D collaboration RD42 at CERN [16]. Charge collection distances up to 300µm have been achieved. Diamond pixel detectors have been built with pixel electronics developed for the ATLAS pixel detector [17] and operated as single-chip modules in test beams (see figure 21). A spatial resolution of 22µm has been measured with 50µm pixel pitch, compared to about 12µm with Si pixel detectors of the same geometry and using the same electronics.

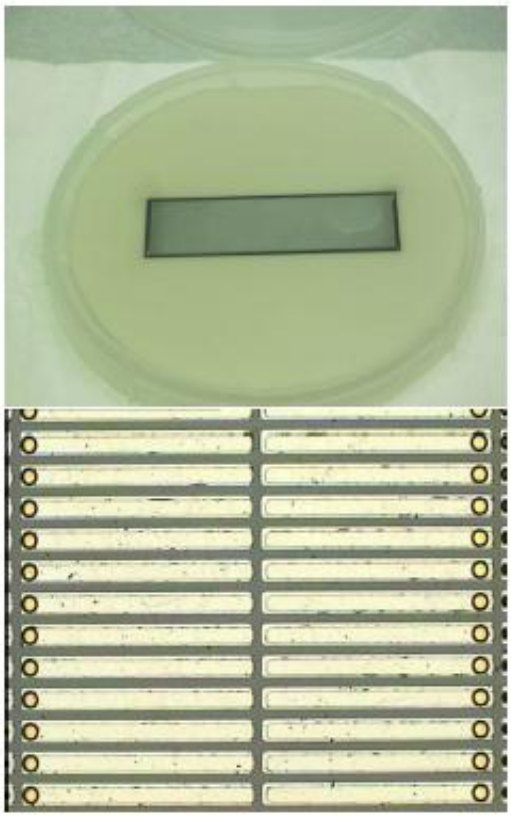

Figure 21. The ATLAS diamond pixel detector [17].

CdTe CdZnTe. Materials, such as CdTe and CdZnTe, have relatively high atomic number and density, and are suitable for x-ray detection (see table 10 and figure 22, 23). They have been used successfully used in small mono-crystalline detectors in diagnostic x-ray energy range for imaging and spectroscopy. Imaging developments are well underway, and CdZnTe arrays with progressively smaller pixels are being tested. At Marshall Space Flight Center (MSFC), for example, devices having 16 x 16 arrays of 300-micron-pitch pixels are currently under evaluation [18]. The problem with CdZnTe has been the charge diffusion within the detector, which limits the spatial resolution. Typical charge-cloud diffusions in 2-mm-thick crystals are ~ 50 – 100 microns.

Material	Z	Bandgap [eV]	Mobility [cm^2/Vs]		Density g/cm^3
			electrons	holes	
Si	14	1.1	1350	480	2.3
Ge	32	0.7	3800	1800	5.3
Diamond	6	5.5	1800	1200	3.5
GaAs	31-33	1.5	8600	400	5.4
AlSb	13-51	1.6	200	700	4.3
GaSe	31-34	2.0	60	250	4.6
CdSe	48-34	1.7	50	50	
CdS	48-16	2.4	300	15	4.8
InP	49-15	1.4	4800	150	
ZnTe	30-52	2.3	350	110	
WSe_2	74-34	1.4	100	80	
BiI_3	83-53	1.7	680	20	
Bi_2S_3	83-16	1.3	1100	200	6.7
Cs_3Sb	55-51	1.6	500	10	
PbI_2	82-53	2.6	8	2	6.2
HgI_2	89-53	2.1	100	4	6.3
CdTe	48-52	1.5	1100	100	6.1
CdZnTe	48-30-52	1.5-2.4			

Table 10. Properties of semiconductors.

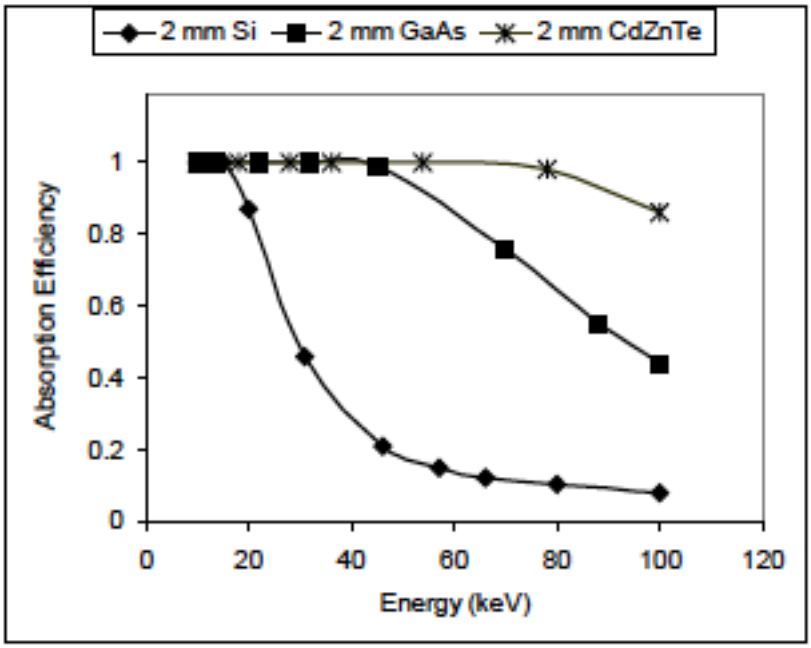

Figure 22. Comparison of the absorption efficiency of 2 mm of CdZnTe, silicon, and gallium arsenide [18].

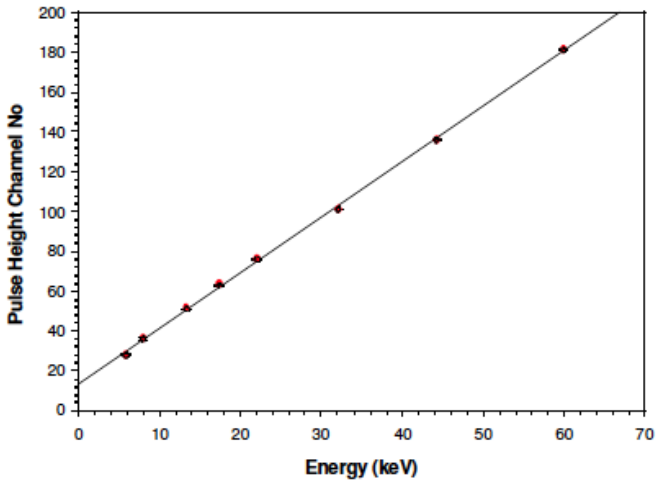

Figure 22 . Results from a 2 mm thick CZT at MSFC [18].

Detector for the future. Poulsen has presented a detector design at an XFEL conference that looks amazing. It is comprised of 2 orthogonal sets of parallel electrodes at 1 μm pitch, on a high-z indium-phosphide substrate [19]. I have not been able to find any supporting documentation for it in the literature. However, given Poulsen's excellent reputation in the community, it is a development to watch. See figure 24.

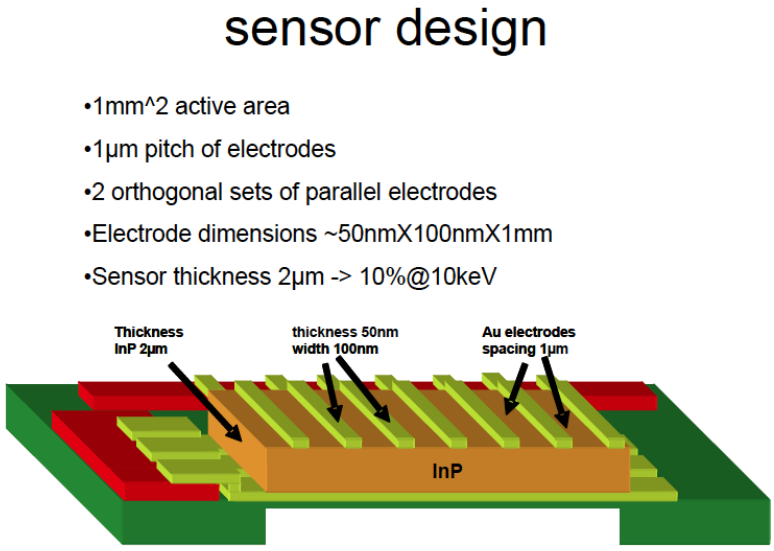

Figure 24. An extremely fine pitch strip detector [19]

Radiation Hardness. Don Brown suggests that for this first class of FFmF experiment, the detector should be as close to the sample as possible, Gunter Muhrer modeled the radiation background of neutrons and gammas in units of

cm^2-eV/s/mA, at two radial positions from the source [20]. In one case, he plots the flux corresponding to a 14-degree opening, corresponding to the cone from a diffraction experiment. In another other case, he plots the flux assuming a 3 cm diameter cylinder, corresponding to the transmission experiment considered in this paper. The results are shown in figure 25 for the neutrons and figure 26 for the gammas.

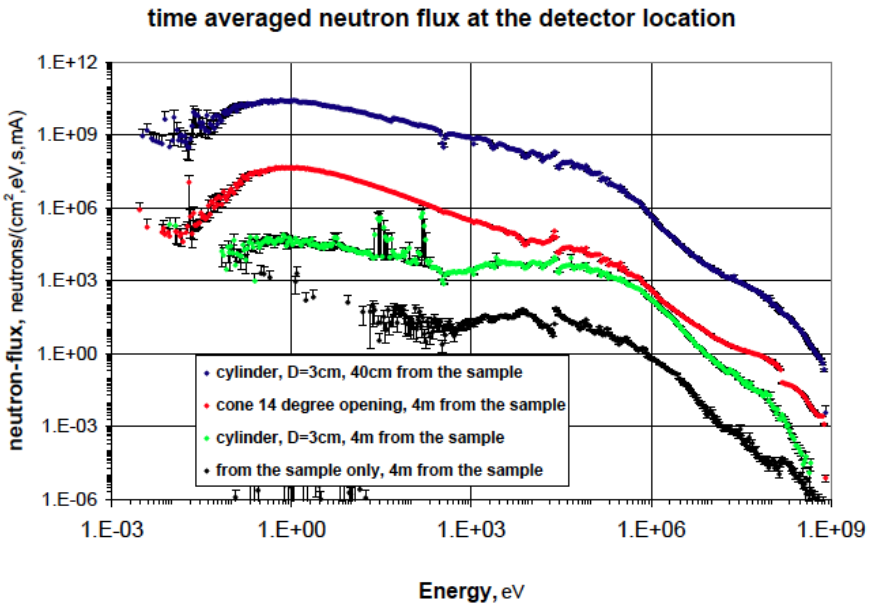

Figure 25. Neutron and gamma flux model at 40 cm.

The total integrated flux of neutrons at a detector positioned 40 cm from the sample, given a 3 cm diameter cylindrical view toward the sample is $1.54x10^{13}$ n/mA/s/cm^2, and for gammas it is $1.54x10^{12}$ gammas/mA/s/cm^2. Low resistivity CMOS would most likely die quickly. High resistivity silicon based detectors might survive 1-10 seconds, and diamond based detectors might survive 10-100 seconds. The gamma background would flood each pixel with approximately 10^6 photons per pixel element per second, assuming a 10 μm^2 pixel. It is fairly evident that a detector cannot be positioned at 40 cm from the sample.

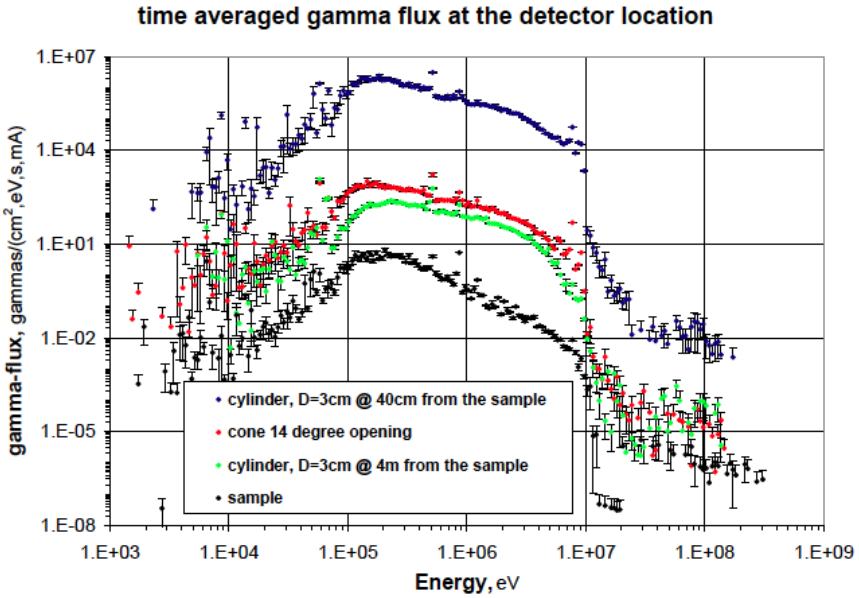

Figure 26. Neutron and gamma flux model at 4 m.

The total integrated flux of neutrons at a detector positioned 4 m from the sample, given a 3 cm diameter cylindrical view toward it, is 1.27×10^9 n/mA/s/cm2, and for gammas it is 4m 2.50×10^8 gammas/mA/s/cm2. Low resistivity CCDs could last 10 to 100s. [21, 22]. CMOS devices could survive 10^3 to 10^4 seconds (depending on specific hardness design). High resistivity silicon-based detectors could last 10^4 to 10^5 seconds and diamond-based detectors might survive 10^5 to 10^6 seconds. The gamma background is down by 4 orders of magnitude, and is now 250 photons per pixel per second. If one assumes an acquisition gate of 100 ns, then the gamma background would contribute 10^{-5} photons per gate. These conditions may be tolerable.

Radiation damage in semiconductors. Radiation damage can be divided into two main components for semiconductors, surface damage and bulk damage [23]. Surface damage usually occurs in oxide layers and causes shifts in the reference voltages in CMOS devices, or in increased noise current in high resistivity silicon detectors. Bulk damage is a nuclear effect resulting in damage clusters. This effect usually results in trapping and a loss of collected signal, increased noise, and the need for increasingly higher depletion voltage.

CCD radiation hardness. Jim Brau did a post-mortem study on the SLD detector at SLAC and reports that CCDs are much more sensitive to radiation damage than other types of semiconductor particle detectors [21]. According to Brau, "Signal charge packets travel longer path before being registered, and the readout method (moving signal row by row from the image area into the output register, with a subsequent shift in the output register to the output node) increases the time a

signal is subject to loss. Furthermore, a much smaller signal is generated in the CCD-based detector (about 1600 electrons of charge) than in other detectors. These factors lead to a radiation tolerance for CCD-based detectors of about 10^9–10^{10} neutrons/cm2, while microstrip detectors are expected to work well up to 10^{14} neutrons/cm2." In a separate study on the same detector, Cris Damerell reported that gamma radiation, on the other hand, resulted in negligible radiation damage to the CCDs [22].

Bebek at LBNL has reported that P-channel, backside illuminated silicon CCDs that were developed and fabricated on high-resistivity n-type silicon were found to be more radiation tolerant than conventional n-channel devices. He irradiated up to 10^{11} 12 MeV protons/cm^2 without killing the device [24].

Silicon and Diamond radiation hardness. Research on the radiation damage effects to high resistivity silicon and diamond-based detectors has been carried out for decades. Although there are some variations in processing that can make a particular device more or less radiation hard, the numbers are fairly consistent. A high resistivity silicon detector can be expected to survive 10^{13} to 10^{14} 1MeV-equivalent neutrons/cm^2 total fluence. For diamond, the tolerable fluence is one order of magnitude higher, or 10^{14} to 10^{15} 1 MeV-equivalent neutrons/cm^2 [27]. For reference, the damage constant for 1 MeV neutrons is roughly twice that for minimum ionizing protons.

CdZnTe radiation hardness. In a study out of the Jet Propulsion Lab, experimenters irradiated 3 mm thick CdZnTe detectors with a) 200 MeV protons up to 5 x 10^9/cm^2), b) thermal and 1 MeV neutrons (up to 10^{11}/cm2), and c) with 5 MeV alphas (up to 10^9/cm^2). The main damage effects at these levels of dose were resolution broadening and charge loss [25]. See table 10.

TABLE III
COMPILATION OF CDZNTE RADIATION DAMAGE STUDIES [15,16]

Radiation / Energy	*Effects*
Proton, 200 MeV	10^9 p/cm^2, 2-4% gain shift 5.10^9 p/cm^2, 13-15% gain shift, factor of two increase in FWHM.
Proton, 200 MeV	5.10^9 p/cm^2, 25% gain shift in strip detector 5.10^9 p/cm^2, 50% gain shift in planar detector
Proton, 200 MeV	5.10^9 p/cm^2, 10% gain shift in strip detector
Proton, 1.3 MeV	10^{10} p/cm^2, interstrip leakage increases 10^{12}p/cm^2, bulk leakage increases 2-3 times
Neutrons, thermal and MeV	10^{11} n/cm^2, factor of two increase in FWHM and measurable charge loss
Alpha, 5 MeV	$2.5.10^9$ α/cm^2, start of charge loss effects $1.5.10^{10}$ α/cm^2, 60% increase in FWHM

Table 10. Results of irradiation studies at JPL [25].

CMOS electronics (ASICS) radiation hardness. There are radiation hardened CMOS processes, some of which are held confidential by the military. In general, a CMOS electronics device is more susceptible to x-ray and gamma ray dose than it is to bulk damage by neutrons and protons. Speiler reports that doses from 10 to 100 Mrad can be tolerated in specially hardened CMOS processes [6].

Scintillators and Phosphors radiation hardness. The damage effect for scintillators is, in general, the creation of color centers, which worsens the light transmission of the material. The scintillation efficiency and conversion efficiency can also be affected in some crystals by radiation damage. The type and the amount of damage are highly dependent on several factors including, the specific crystal or phosphor, the impurity concentration, the dose rate and the temperature (see table 11) [26]. A full review of FFmF candidate scintillators and their relative radiation hardness was beyond the scope of this initial detector survey.

	Inorganic crystals	Organic scintillators
damages	mainly in colouring (transmittance)	mainly in scintillation efficiency. Colouring to some extent in plastics
γ-rays versus hadrons	larger damage for hadrons 10-100 times	similar in magnitude
recovery in time	yes (spontaneous, thermal, UV annealing)	almost absent
Radiation hardness	depends largely on crystals	similar level at 10^{4-5} Gy

Table 11. Introduction to scintillators, M. Kobayashi [25].

Detectors that require a revolutionary leap from present day performance. Poulsen has reported on a process to imbed columns of CsI into a silicon substrate. As stated above, 1-2 mm of CsI has relatively good absorption efficiency for photons up to 350 keV. In Poulsen's design, the silicon substrate is an inactive material, there just to support the scintillator and to prevent crosstalk. A 3D high resistivity detector has a similar vertical column implanted as an electrode that could be used to collect the light emission from the CsI. Combining Poulsen's concept with a 3D silicon or diamond detector into a single integrated detector is a provocative and undeveloped idea. The progress in the performance of diamond has been steady. The high energy physics community is very involved, and this community will spearhead development over the next 3-5 years, driven by the needs of the next generation LHC detectors.

Detectors that require extensive evolutionary development. Detection systems based on scintillator or phosphor converters that are optically coupled to CCDs are in a mature state of development and their operation is well understood. However, absorption efficiency for thin high-resolution phosphors at the very hard incident x-ray energies at FFmF is extremely low. In figure 27, plots of absorption thickness as a function of photon energy for some select phosphors. The required thickness for photons above 20 keV is off the chart into a region of thickness where the spatial resolution contribution from the phosphor or scintillator is unacceptable.

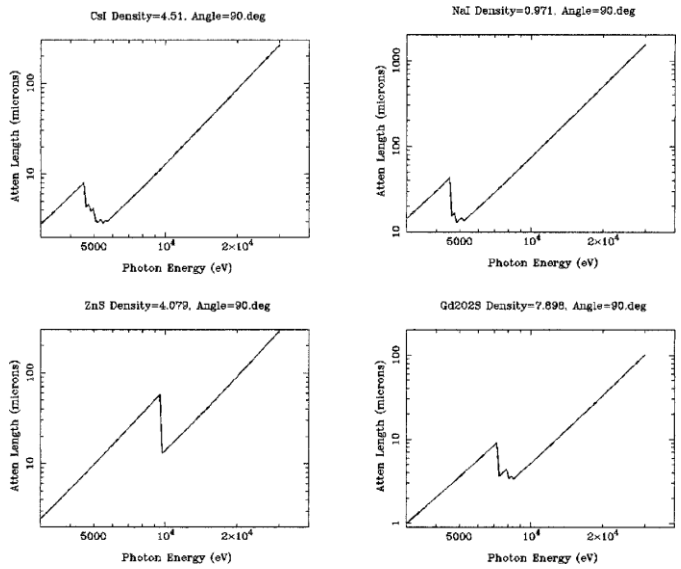

Figure 27. Absorption efficiency curves for some select phosphors.

Commercially available CCDs are not radiation hard to neutrons at the level required for operation at FFmF. Optical coupling schemes need to, be developed to remove the CCD from the path of the primary beam and to where the radiation environment is reduced or can be effectively shielded against. Good quality CCDs range in cost from $10k-$100k each. A custom mask set costs on the order of $200k.

CdZnTe is very efficient for stopping x-rays, as is shown in figure 6. However, the diffusion cloud produced by the x-ray absorption is 10 x the required spatial resolution for FFmF. Work on these detectors is ongoing, both to improve the resolution and to get to smaller pixels. The commonly held wisdom in the detector community is that the limitations to the performance are largely due to the intrinsic materials and its processing. Significant improvements are considered a long shot.

Detectors that require some evolutionary development. Structured plates of CsI, or CsI light guides as described by Poulsen, present a way to get reasonable efficiency (10^{-2}) (figure 6), and preserve good spatial resolution (μm's). Two alternatives to CCD readout of these crystals are high resistivity silicon detectors

and diamond-based detectors. The penetration depth of the 550 nm light output from CsI is only on the order of 5-10 μm in these materials. In silicon, the SiO2 layer may be thick enough to absorb the light before it enters the active detector volume. R&D on so-called "thin window" processes is required to develop a successful means to couple CsI light output efficiently to either of these detector types.

Semiconductors have sufficient density to convert an incident x-ray directly, up to a certain energy depending on thickness. High resistivity silicon detectors are not as efficient a converter as CdZnTe, however, their conversion efficiency is much higher than scintillator or phosphor. The charge pairs (electrons and holes) drift to opposite-side electrodes under the influence of an electric field. Charge integrating electronics are connected directly to the electrode pads with wire bonds or pixels. This is the basic structure of the PAD. The spatial resolution does not depend on the semiconductor thickness and so the detectors can be stacked in multiple layers without loss of resolution. Silicon detectors are a very mature technology in terms of understanding the operational characteristics and radiation damage effects. Diamond is an attractive alternative with an order of magnitude better radiation hardness than silicon.

The uncertainty in the imaging performance of semiconductors as direct x-ray converters and detectors is the multiple scattering of the secondary electron produced in the Compton process. The conversion and scattering through the silicon needs to be fully simulated to determine if this is a fundamental limitation to the spatial resolution of these types of detectors.

A large number of ASICS have been developed specifically for silicon detector readout. These have mostly been in CMOS processes, which provide low noise amplification, signal processing, and high-speed readout for microstrips and pixels in a mature and now standard 0.25 μm foundry process. There is a lot of experience in the high energy physics community, and in the Subatomic Physics group at LANL, in high density connections, such as ultrasonic wire bonds, bump bonds, and high-density interconnect circuits, the essential components that provide connectivity from detector to electronics. Eventually, an ASIC will have to be custom designed specifically for the detector that is built.

Some basic R&D Costs. Silicon detector mask sets cost $50-$100k per design. The sensors cost anywhere from $0.5k-$10k each, depending on the thickness and design complexity.

CMOS ASIC mask sets in the currently standard 0.25 μm process cost approximately $100k per design. Wafer production runs require minimum orders if 12 8-inch wafers and that costs an additional $100k. Prototype multiuser runs are available through MOSIS and provide a means to develop a design and get a handful of chips back each time to test. This type of run costs between $25-$50k. The number of ASIC chips on a production wafer or on a multiuser prototype reticle simply depends on

the size of the individual chip and the available processing area on the wafer.

The 0.25 μm process might be small enough to design the electronics to match a pixel element as small as 20 μm^2. This depends on the complexity or number of transistors in the circuit design. A smaller feature size process is almost certainly required for pixels that are smaller than that. The Taiwan Semiconductor Manufacturing Company (TSMC) CMOS fabrication processes available through MOSIS (the standard American ASIC broker), range from 40 nm to 0.35 μm. The cost of smaller feature size processes escalates rapidly, as is shown if figure 28 [28]. The smaller processes allow matching to smaller pixels, radiation tolerance generally scales favorably with smaller feature sizes, and device speed increases as well (figure 29). The software design tools and the engineering expertise to go to smaller feature sizes are not as readily available as they are for the 0.25 μm process.

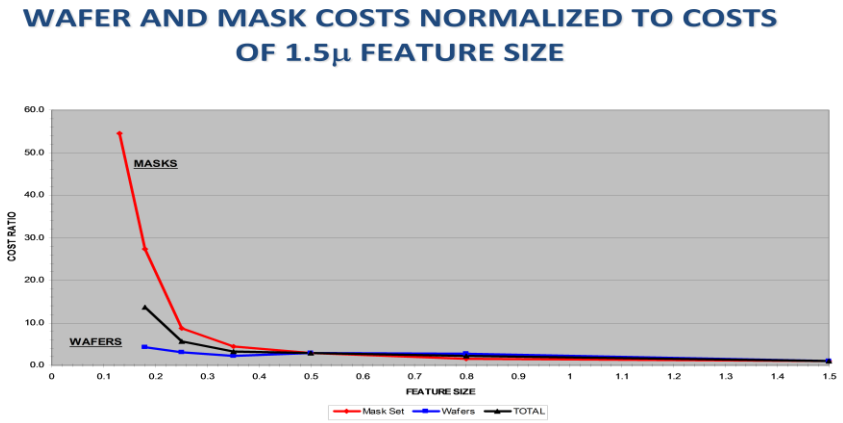

Figure 28. Older data, but the trend is still relevant.

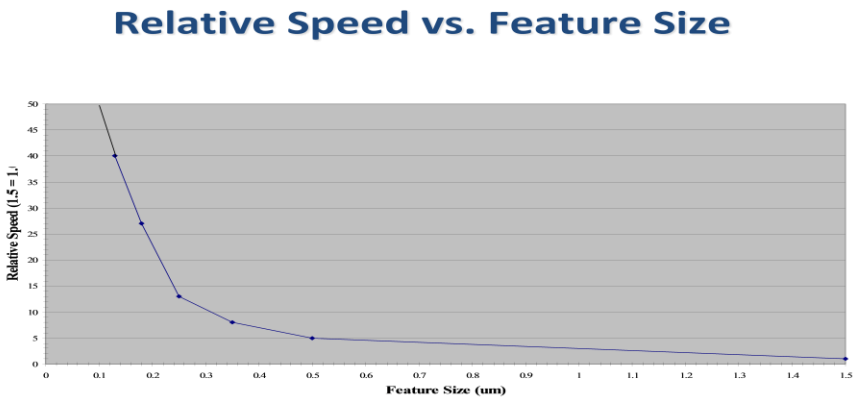

Figure 29. Speed versus minimum feature size.

A near-term task list (1-4 years).

1. Procure the most relevant PAD detectors of an existing design that is available. Characterize the performance with x-rays. Perform radiation damage studies with neutrons and gammas.
2. Perform detailed simulation of x-ray conversion and secondary electron scattering and electrode charge collection for a high resistivity silicon pixel detector.
3. Perform a survey of existing ASICs designs and identify those that are appropriate and available for testing new detector concepts.
4. Evaluate "thin window" silicon detector options, first by analysis and simulation, and if those results are positive, design and procure prototype detectors. Test performance with structured CsI converter.
5. Evaluate scintillator converter options, in particular, structured CsI. Perform X-ray conversion and radiation damage test with neutrons and gammas.
6. Monitor developments in Poulsen's concept of embedded CsI columns. Explore technical feasibility of an integrated embedded CsI-silicon detector. Perform simulations to model potential performance.
7. Monitor developments in Poulsen's InP double-sided strip detector concept.
8. Monitor diamond detector development, especially LHC.
9. Monitor CdZnTe developments.
10. Establish collaborative relationships with appropriate outside research groups.

References

1. X-RAY DATA BOOKLET, Center for X-ray Optics and Advanced Light Source, Lawrence Berkeley National Laboratory
2. "X-ray imaging with submicrometer resolution employing transparent luminescent screens," Andreas Koch et. al., J. Opt. Soc. Am. A/Vol. 15, No. 7/July 1998
3. "Scintillation detectors for x-ray," Martin Nikl, Meas. Sci. Technol. 17 (2006) R37-R54
4. "Fast Microtomography Using High Energy Synchrotron Radiation," Marco Di Michieli et. al., Review of Scientific Instruments 76, 043702 (2005)
5. "Charge-coupled device area array detectors," Sol M. Gruner et. al., Review of Scientific Instruments, Volume 73, Number 8, Aug 2002
6. "Imaging Detectors and Electronics – A View of the Future," Helmuth Spieler, IWORID 2003, Riga, Latvia, September 7-11, 2003 LBNL

7. "A high spatial-resolution three-dimensional detector array for 30-200 keV X-rays based on structured scintillators," U.L. Olsen, S. Schmidt and H.F. Poulsen, J. Synchrotron Rad. (2008) 15, 363-370
8. "A mixed analog and digital pixel array detector for synchrotron x-ray imaging," Daniel R. Schuette, Doctoral Dissertation, Cornell University, August, 2008
9. A. Madsen, Plenary remarks, Materials **I**maging and **D**ynamics Workshop ESRF, Grenoble, October 28-29, 2009
10. "Large-format, high-speed, X-ray pnCCDs combined with electron and ion imaging spectrometers in a multipurpose chamber for experiments at 4th generation light sources," Lothar Struder et. al., Nucl. Instr. Meth. A 614, (2010) 483–496
11. S.I. Parker, C.J. Kenney and J. Segal, 3D — A proposed new architecture for solid-state radiation detectors, Nucl. Instrum. Meth. **A 395** (1997) 328.
12. "Development of 3D detectors featuring columnar electrodes of the same doping type," C. Piemonte et. al., Nucl. Instr. Meth. A541 (2005) 441
13. SINTEF, Strindveien 4, Trondheim, Norway
14. "Detection of x-ray and gamma-ray photons using silicon diodes," Carrol/Ramsey, Detection Technology Inc. Micropolis, Finland, 2000
15. "The European XFEL Project," Ulrich Trunk, Photon-Science Detector Group, Deutsches Elektronen-Synchrotron DESY, Hamburg, Germany
16. Rd42 Collaboration, CERN, Geneva, Switzerland
17. "Diamond Detectors in High Radiation Environments," Harris Kagan, Ohio State University Advanced Instrumentation Seminars, Sept. 5, 2007, SLAC
18. "Characteristics of a 16x16 Fine-Pixel Cadmium-Zinc-Telluride Detector," D.P.Sharma et. al, Report for the Marshall Space Flight Center
19. "Case for studies of bulk materials at XFEL," Henning Friis Poulsen, Mid-Workshop 2009, ESRF Grenoble
20. Gunter Muhrer, LANSCE-LC, LANL, private communication.
21. "Investigation of Radiation Damage Effects in Neutron Irradiated CCD," James E. Brau, Nucl. Instr. Meth. A, 549 (2005) 117-121
22. "Radiation Damage in CCDs used as Particle Detectors," C. J. S. Damerell Rutherford Appleton Laboratory, Chilton, Didcot, OX11 0QX, England February 1997
23. " Radiation damage in silicon detectors," Gunnar Lindstrom, Nucl. Instr. Meth. A, 512 (2003) 30-43
24. "Proton radiation damage in P-channel CCDs fabricated on high-resistivity silicon," C. Bebek et. al., escholarship.org/uc/item/9dg729jz, 2002
25. "Radiation Effects in CdZnTe Gamma-Ray Detectors Produced by 199 MeV Protons," Larry S. Varnell et. al., Presented at SPIE Technical Conference, 5-7 August 1996 Denver, Colorado
26. "Introduction to scintillators," M. Kobayashi, KEK (Japan) report, 17 November, 2003
27. RD50 Collaboration for Radiation Hardness in Semiconductors, CERN, Geneva Switzerland
28. "MOSIS Overview", Cesar A. Pina, presentation, October, 2003